Available online at www.sciencedirect.com
SCIENCE DIRECT®
Inorganica Chimica Acta 358 (2005) 2891–2899
Inorganica Chimica Acta
www.elsevier.com/locate/ica

A nitric oxide releaser based on the μ-oxo-hexaacetate-bis(4-methylpyridine)triruthenium nitrosyl complex

Henrique E. Toma [a,*], Anamaria D.P. Alexiou [a], André Luiz B. Formiga [a], Marcelo Nakamura [a], Sergio Dovidauskas [a], Marcos N. Eberlin [b], Daniela M. Tomazela [b]

[a] *Instituto de Química, Universidade de São Paulo, Caixa Postal 26077, CEP 05513-970, São Paulo, SP, Brazil*
[b] *Instituto de Química, Universidade Estadual de Campinas UNICAMP, Campinas, Brazil*

Received 24 June 2004; accepted 7 August 2004
Available online 18 September 2004

Dedicated in memory of Professor Rex Shepherd

Abstract

The properties of the trinuclear cluster $[Ru_3OAc_6(pic)_2(NO)]PF_6$ (pic = 4-methyl pyridine, Ac = acetate ion) and the photochemical behavior of the corresponding molecular films are reported in this paper. In this compound, the unpaired π* electron from NO and the unpaired electron from the π-orbitals of the Ru_3O unity are strongly coupled; as a consequence, the changes in electronic distribution associated with the several successive redox states promote dramatic effects in the spectroscopic and electrochemical properties of the nitric oxide ligand and the entire complex. NO release has been observed by light irradiation ($\phi = 0.038$ at 365 nm and $\phi = 0.019$ at 468 nm, in acetonitrile solution), changing the original violet color into deep blue. The same behavior has been observed in solid state and in PVA films incorporating this compound, revealing its potential usefulness as NO photoreleaser, as well as for the monitoration of light exposure intensities.

Keywords: Oxo-ruthenium clusters; Ruthenium acetate clusters; Trinuclear ruthenium clusters; Nitric oxide; Nitrosyl complexes

1. Introduction

In recent years, a great number of reports dealing with NO activity in biological systems have been published [1–8] and ruthenium complexes have been studied as scavengers of NO, or reciprocally, their nitrosyl complexes have been investigated as NO delivery systems toward biological targets [9–24]. In this field, important contributions have been made by Shepherd and coworkers [25–32], specially in the design and evaluation of a number of new transition metal complexes as NO carriers for biological applications.

It should be noticed that nitric oxide is a non-innocent ligand which can coordinate to a metal center yielding either a linear or a bent MNO geometry [33–36], assuming three possible oxidation states: NO^+, NO^0 or NO^- [37]. Therefore, the NO behavior is rather puzzling, since in the NO^+ form the ligand is a very strong π-acceptor and would prefer metal ions in low oxidation states, but in the NO^0 form it can combine with metal ions either in intermediate or high oxidation states, remaining formally in the neutral form or converting into NO^+ by reducing the metal center. On the other hand, NO can also be converted into NO^- species, under more reducing conditions.

* Corresponding author. Tel.: +55 11 3818 3887; fax: +55 11 3815 559.
E-mail address: henetoma@iq.usp.br (H.E. Toma).

0020-1693/$ - see front matter © 2004 Elsevier B.V. All rights reserved.
doi:10.1016/j.ica.2004.08.004

Because of the systematic changes in the electronic properties for the several successive oxidation states, the triangular ruthenium acetate clusters $[Ru_3O(CH_3CO_2)_6L_3]^n$ (L = H_2O, N-heterocyclic, etc.) [38] provide rather unique species to interact with NO, as we reported in our preliminary work on the $[Ru_3O(CH_3CO_2)_6(py)_2(NO)]PF_6$ complex [39]. In this system, the strong interaction between the unpaired π* electron from NO and the unpaired electron from the π-orbitals of the $(Ru^{III,III,III})_3O$ unity is responsible for its pronounced NO^0 character, as evidenced by the vibrational and spectroelectrochemical data. Here, in order to enhance the NO^0 character further, the pyridine ligand was replaced by the 4-methyl pyridine (picoline) analogue (Fig. 1), and a full characterization of the complex was carried out by means of mass spectrometry, spectroscopy, electrochemistry, spectroelectrochemistry and scanning probe microscopy. Due to its higher basicity, the picoline ligand is expected to decrease the electron acceptor properties of the $(Ru^{III,III,III})_3O$ unity, diminishing the extent of electron donation from the NO ligand. In addition, NO release was observed under UV–Vis light irradiation, changing the complex from original violet color into deep blue. This effect was also probed at the nanoparticle level by means of MAC mode atomic force microscopy, revealing intriguing morphology changes accompanying the NO release.

2. Experimental

2.1. Materials

Tetraethylammonium perchlorate ($TEAClO_4$) [40] and the starting complex $[Ru_3O(CH_3CO_2)_6(pic)_2(CH_3OH)]PF_6$ were prepared as previously described in the literature [41]. Acetonitrile (HPLC grade, Aldrich) was kept in the presence of 3 Å molecular sieves.

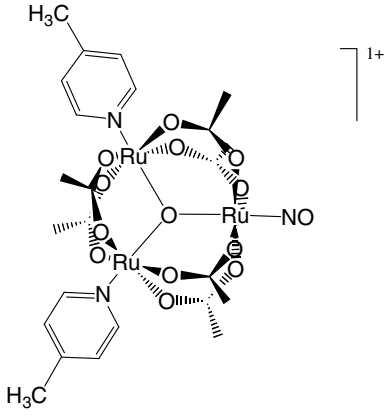

Fig. 1. Structural representation of $[Ru_3O(CH_3CO_2)_6(pic)_2(NO)]^+$.

2.2. Synthesis of $[Ru_3O(CH_3CO_2)_6(pic)_2(NO)]PF_6$

Dichloromethane, 50 mL, containing 0.52 g $[Ru_3O(CH_3CO_2)_6(pic)_2(CH_3OH)]PF_6$ was saturated with Ar for 20 min, then with NO for 35 min and finally with Ar for 60 min. After this, the product was precipitated by adding petroleum ether. The violet solid was collected on a filter, washed with petroleum ether and dried under vacuum. Yield: 72%. Elemental *Anal.* Calc. for $C_{24}H_{32}F_6N_3O_{14}PRu_3$: C, 27.86, H, 3.12, N, 4.06. Found: C, 27.52; H, 3.27; N, 4.18%.

2.3. Physical measurements

Infrared spectra were recorded on a Shimadzu FT-IR model 8300 spectrophotometer.

^1H and ^{13}C NMR spectra and two dimensional COSY (^1H, ^1H) and HMQC (^1H, ^{13}C) were recorded on Varian INOVA1 300 MHz or Bruker DRX 500 spectrometers, using 10^{-2} mol L^{-1} cluster solutions in CD_3CN. The reported chemical shifts were relative to residual protons of solvent.

The electronic spectra were recorded on a Hewlett–Packard model 8453 diode-array spectrophotometer, using 295 nm UV cut-off filters. Cyclic voltammetry and spectroelectrochemistry were carried out with an EG&G Instrument, consisting of a model 283 galvanostat/potentiostat. A conventional three electrodes electrochemical cell was used with platinum disk as working electrode, a Luggin capillary arrangement with an Ag/$AgNO_3$ (0.01 mol L^{-1}) reference electrode in 0.10 mol L^{-1} $TEAClO_4$ (tetraethylammonium perchlorate) in acetonitrile and a platinum wire as auxiliary electrode. UV–Vis spectroelectrochemistry was conducted using a rectangular quartz cell of 0.025 cm internal optical path length, containing an optically transparent gold minigrid electrode, a platinum wire and a small Ag/$AgNO_3$ electrode as a working, auxiliary and reference electrodes, respectively. FT-IR spectroelectrochemical measurements were carried out in acetonitrile solution containing 0.1 mol L^{-1} $LiClO_4$, using a homemade IR-TRAN® cell and a transparent gold minigrid electrode.

Mass spectrometric measurements were performed using a high-resolution hybrid quadrupole (Q) and orthogonal time-of-flight (Tof) mass spectrometer (Q-Tof from Micromass, UK) operating in the positive ion electrospray ionization mode. The temperature of the nebulizer was 200 °C and the cone voltage was 40 V. Tandem mass spectrum (MS/MS) was acquired using the product ion scan mode via mass-selection of the singly charged complex, its collision-induced dissociation (CID) with N_2 at 15 eV energy, and high-resolution orthogonal Tof mass analysis of the CID ionic fragments.

Photolysis of 10^{-4} mol L^{-1} of cluster solutions in CH_3CN was carried out using a 150 W Xenon Arc

Lamp and an f/3.4 Monochromator (Applied Photophysics). Absorbed light intensities were determined by ferrioxalate actinometry. $[Ru_3OAc_6(pic)_2(NO)]PF_6$ films in polyvinyl alcohol matrix were prepared using a procedure described in the literature [42] and their electronic spectra were obtained using a Guided Wave, model 260 fiber optics spectrophotometer.

Scanning probe microscopy (SPM) images were obtained with a PicoSPM I Molecular Imaging instrument in the magnetic AC (MAC) mode, employing MAClever Type II ($k = 2.8$ N m^{-1}, $f \sim 60$ kHz) operating in an amplitude set point 4.4 V at room temperature. Molecular films of the nitrosyl-cluster were prepared by evaporating a micro volume of a methanolic solution of the nitrosyl cluster onto high graded mica, in a clean room, under artificial light illumination. The MAC mode AFM images were obtained with scan rate at 3 Hz and 512 points per line.

2.4. Theoretical calculations

Geometry optimization was performed by starting from a molecular mechanics structure, and employing the PM3 method as implemented in HYPERCHEM program, using a convergence criterion of 10^{-5} kcal mol^{-1} for SCF and 10^{-3} kcal mol^{-1} Å^{-1} for geometry optimization, by the conjugated gradient method. Molecular orbital and spectra calculations were carried out with the ZINDO/S method, using the default parameters and 10^{-7} kcal mol^{-1} as convergence criterion. An active space of 20 frontier molecular orbitals (10 occupied and 10 unoccupied) was used for configuration interaction using single excitations.

3. Results and discussion

3.1. ESI spectra and CID pattern

The positive ion ESI mass spectrum of the $[Ru_3O(CH_3CO_2)_6(pic)_2(NO)]PF_6$ complex in methanol:water solution is shown in Fig. 2(a). In the electrospray positive ion mode, the complex can be directly transferred by ESI to the mass spectrometer and can be detected as a multicomponent structure of isotopomeric ions; the most abundant ion being that of *m/z* 891. Ru possesses seven isotopes: ^{104}Ru (18.7%), ^{102}Ru (31.6%), ^{101}Ru (17.0%), ^{100}Ru (12.6%), ^{99}Ru (12.7%), ^{98}Ru (1.88%), and ^{96}Ru (5.52%).

The CID pattern of $[Ru_3O(CH_3CO_2)_6(pic)_2(NO)]^+$ shown in Fig. 2(b) reveals that the picoline ligand is preferentially released (81%) from the complex, as expressed by the peak at *m/z* 798 associated with the $[Ru_3O(CH_3CO_2)_6(pic)(NO)]^+$ ion. Dissociation of the NO ligand is much less efficient, as shown by the $[Ru_3O(CH_3CO_2)_6(pic)_2]^+$ peak at *m/z* 862 (11%) and

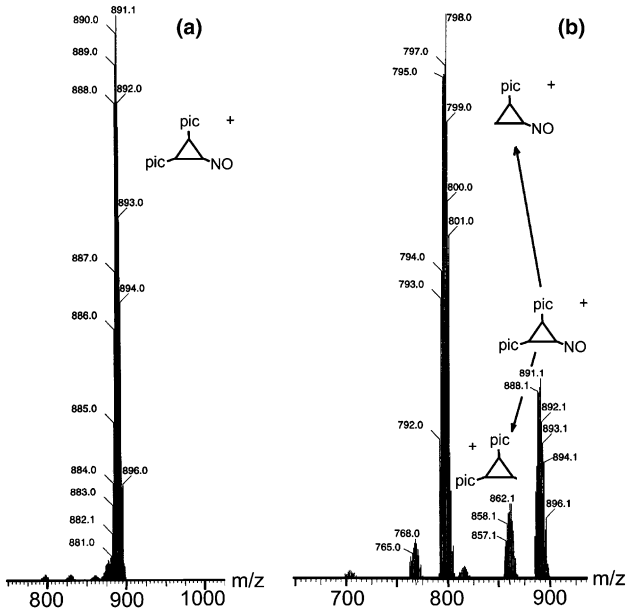

Fig. 2. (a) Positive ion ESI mass spectrum for a methanol:water solution of $[Ru_3O(CH_3CO_2)_6(pic)_2(NO)]^+$. (b) Tandem product ion mass spectrum for the mass-selected ionic cluster of $[Ru_3O(CH_3CO_2)_6(pic)_2(NO)]^+$ centered at *m/z* 891.

the $[Ru_3O(CH_3CO_2)_6(pic)]^+$ peak at *m/z* 768 (5%). It is interesting to note the existence of picoline free $[Ru_3O(CH_3CO_2)_6NO]^+$ species at *m/z* 705, although in very small amount (1%). These results indicate a stronger Ru–NO bond, in comparison with the Ru-picoline bond.

3.2. EPR spectra

The EPR spectra of the complex at 77 K do not exhibit any detectable signal, in spite of the fact that the precursor cluster $[Ru_3O(CH_3CO_2)_6(pic)_2(CH_3OH)]PF_6$ and the NO ligand are paramagnetic species. Therefore, a strong interaction between the species should be occurring in the complex.

3.3. ^{1}H- and ^{13}C NMR spectra

The ^{1}H- and ^{13}C NMR spectra of the cluster (Table 1) were assigned by comparison with related clusters [43–53], and using peak integration in addition to COSY (^{1}H, ^{1}H) and HMQC (^{1}H, ^{13}C) bidimensional techniques (not shown). The signals of the ligand coordinated to Ru_3O core are dependent on the oxidation states of the ruthenium ions. Reduced clusters containing Ru ions in the III, III, II formal oxidation states usually show coordinated ligand signals near those of the free molecules, only slightly downfield shifted. On the other hand, the oxidized clusters (III, III, III) are paramagnetic and the signals are influenced by the inductive effects from the metal center and the paramagnetic anisotropy to the Ru_3O unit [48]. The data analysis (Table 1) indicated

Table 1
^{1}H and ^{13}C chemical shifts (ppm) for the $[Ru_3O(CH_3CO_2)_6L_3]PF_6$ (Ru_3L_3) clusters in CD_3CN

		$Ru^{III,III,III}pic_2(MeOH)$[a]	$Ru^{III,III,III}py_2NO$[b]	$Ru^{III,III,III}pic_2(NO)$	$Ru^{III,III,II}(CO)pic(THF)$[c]
^{1}H	H_3C (Ac)	4.70 (12 H)	3.96 (12H)	3.73 (12H)	1.97 (6H)
		6.33 (6H)	3.28 (6H)	3.11 (6H)	1.95 (6H)
					1.73 (12H)
	$H_{2,6}$ (L)	−1.58 (4H)	4.49 (4H)	4.82 (4H)	9.43 (2H)
	$H_{3,5}$ (L)	4.89 (4H)	8.18 (4H)	8.01 (4H)	8.10 (2H)
	H_3C (L)	2.88 (6H)		4.98 (6H)	2.82 (3H)
^{13}C	H_3C (Ac)		9.1	10.1	
			16.4	17.1	
	COO^{2-}		221.2	219.8	
	$C_{2,6}$ (L)		162.1	160.3	
	$C_{3,5}$ (L)		113.7	114.5	
	C_4 (L)		152.4	166.2	
	H_3C (L)			16.4	

[a] Ref. [55].
[b] Ref. [39].
[c] Ref. [56].

that the proton signals of CH_3 (acetate) and H_2 (picoline) are in between the signals of diamagnetic and paramagnetic clusters. This can be ascribed to the effect of NO coordination, which increases the electronic density on the Ru_3O center, decreasing the paramagnetic effects. The increase in the π density is reflected in the J values of pyridine ring signals ($^{3}J_{2,3}$ = 6.1 Hz). It should be noticed that in typical oxidized clusters, the scalar constants are too small to be observed because the coupling is reduced as the oxidation state of the coupled nucleus increases [54].

3.4. FT-IR spectra

The main feature in the FT-IR spectrum (Fig. 3) is the vibrational peak at 1874 cm^{-1}, very close to that for free NO (1876 cm^{-1}), and as expected, slightly higher than that for the analogous pyridine derivative [39], i.e., ν(NO) = 1865 cm^{-1}. The remaining peaks are associated with the characteristic vibrations of acetate and the PF_6^- species; the most relevant ones were indicated in Fig. 3.

3.5. Electronic Spectra

The electronic spectrum of $[Ru_3O(CH_3CO_2)_6(pic)_2(NO)]PF_6$ (Fig. 4) consists of at least four bands at 690 nm ($\varepsilon = 1.20 \times 10^3$ cm^{-1} mol^{-1} L), 540 nm (2.42×10^3 cm^{-1} mol^{-1} L), 460 nm (2.67×10^3 cm^{-1} mol^{-1} L) and 360 nm (3.30×10^3 cm^{-1} mol^{-1} L). Because of the expected influence of the strong Ru–NO bond in the properties of the nitrosyl complex, a careful computational work has been carried out, starting from a geometry generated by molecular mechanics and

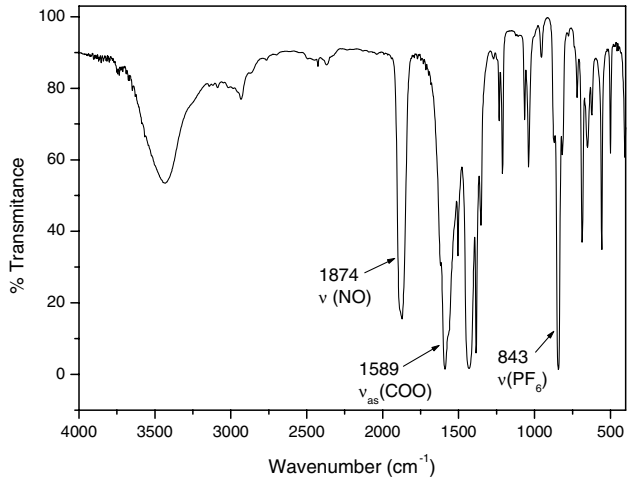

Fig. 3. FT-IR spectrum of the $[Ru_3O(CH_3CO_2)_6(pic)_2(NO)]PF_6$ cluster.

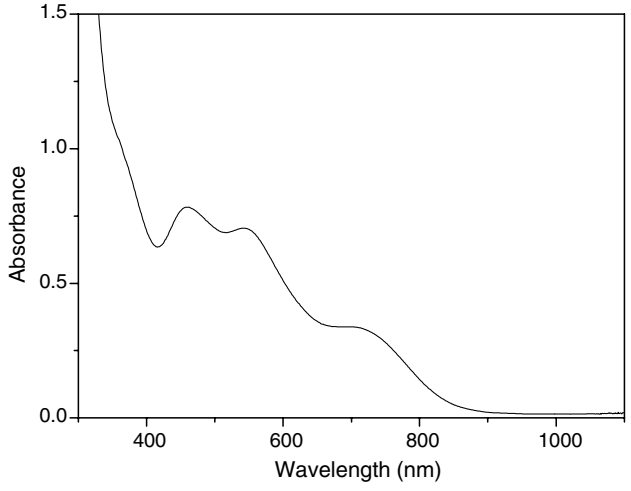

Fig. 4. Electronic spectrum of $[Ru_3O(CH_3CO_2)_6(pic)_2(NO)]PF_6$ (10^{-3} mol L^{-1}) in acetonitrile.

Table 2
ZINDO/S (CIS) molecular orbital composition (%) for $[Ru_3O(CH_3CO_2)_6\ (4\text{-pic})_2(NO)]^+$

MO	Energy[a]	Ru	μ-Oxo	NO	pic	$CH_3CO_2^-$
130	−2.49	19.49	4.81	1.54	71.62	2.53
129	−2.72	4.57	0.00	0.00	94.90	0.52
128	−3.34	31.65	4.25	51.91	10.81	1.38
127	−3.52	35.11	0.57	62.08	0.23	2.01
126 (LUMO)	**−4.46**	**52.43**	**12.82**	**11.41**	**20.69**	**2.65**
125 (HOMO)	**−8.61**	**81.46**	**0.00**	**0.00**	**14.57**	**3.97**
124	−9.75	77.30	0.12	0.12	0.05	22.41
123	−9.82	84.09	8.00	0.57	2.20	5.14
122	−9.90	88.77	2.17	0.20	2.19	6.67
121	−10.11	79.46	0.19	0.03	0.03	20.29
120	−11.25	73.54	0.01	0.00	0.09	26.36
119	−11.44	43.53	4.69	35.77	3.18	12.83
118	−11.57	45.54	4.41	39.28	1.12	9.65
117	−11.78	0.05	0.00	0.00	98.52	1.44
116	−11.80	0.17	0.03	0.12	99.12	0.56

[a] Unit: eV.

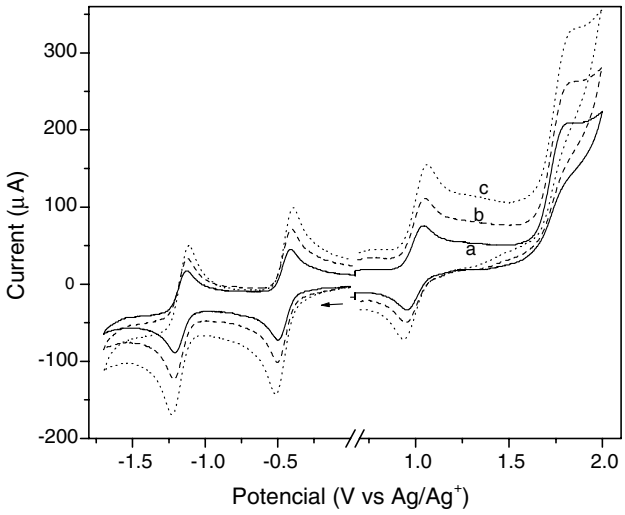

Fig. 5. Cyclic voltammogram of $[Ru_3O(CH_3CO_2)_6(pic)_2(NO)]PF_6$, ($10^{-3}$ mol L^{-1}) in acetonitrile containing 0.1 mol L^{-1} $TEAClO_4$, at scan rates of 50 (a), 100 (b) and 200 mV/s (c).

optimizing using the semi-empirical PM3 method as implemented in the HYPERCHEM-7.1 program. The results from molecular orbital calculations using the ZINDO/S method are summarized in Table 2.

According to the theoretical calculations, there is a strong participation of NO in the HOMO levels, e.g., MO 119 and 118, as well as in the LUMO levels, including MO 126, but specially in MO 127 and 128 (Table 2). ZINDO/S spectral simulations indicated the occurrence of transitions from MO 119 and 118 to MO 127 and 128 above 560 nm, although with very weak intensities. These transitions should be related to the broad band observed at 690 nm in the nitrosyl complex. The calculated HOMO–LUMO transition (MO 125 → MO 126) appeared at 536 nm, corresponding to a very strong band, coinciding with the observed band at 540 nm (Fig. 4). Three less intense bands corresponding to the electronic transitions from MO 120 and MO 125 to MO 127 and MO 128 have been calculated at 525, 508 and 498 nm, but they should be hidden under the envelope of the absorption bands in the 500 nm region (Fig. 4). Another strong band corresponding to the MO 125 → MO 128 transition was theoretically predicted at 466 nm, coinciding with the observed band at 460 nm. Finally, in the 300–400 nm range, the theoretical spectrum is dominated by the electronic transitions from MO 125 to MO 129 and 130, corresponding to Ru_3O → pic charge-transfer bands, as well as by electronic transitions from MO 123, 124 to MO 127, 128, corresponding to Ru_3O → NO charge-transfer bands. All such transitions shoud lead to superimposed bands, under the envelope of the broad absorption profile observed below 400 nm.

Therefore, excitation in the visible–UV region leads to the population of the LUMO 126, 127 and 128 levels, involving a large or predominant participation of NO. This result explains the unusual absorption profile observed in the electronic spectra of the nitrosyl cluster, as compared with the typical examples from the literature [38,57], and will be important for the understanding of its photochemical properties.

3.6. Cyclic voltammetry

Cyclic voltammetry of $[Ru_3O(CH_3CO_2)_6(pic)_2(NO)]^+$ (Fig. 5) exhibits four redox waves at −1.17, −0.45, +1.00 and +1.81 V vs. Ag/Ag^+ associated with the $[cluster]^{-1/0/+1/+2}$ successive redox couples. It should be noticed that in the case of well-behaved systems, such as the tris(pyridine) cluster [14], $[Ru_3O(CH_3CO_2)_6(C_5H_5N)_3]^+$, the difference between successive redox potentials is nearly constant and very close to 1 V, i.e., −1.58, −0.31, +0.71, +1.67 V vs. Ag/Ag^+, corresponding to the Ru^{III} $Ru^{II}Ru^{II}/Ru^{III}Ru^{III}Ru^{II}/Ru^{III}Ru^{III}Ru^{III}/Ru^{IV}Ru^{III}Ru^{III}/Ru^{IV}Ru^{IV}Ru^{III}$ redox couples.

In both cases, the potentials span approximately at 3 V range. However, in the case of the nitrosyl complex, the differences between the successive potentials are not regular, i.e., 0.72, 1.45 and 0.81 V, as compared with 1.27, 1.02, 0.96 V for the tris(pyridine) cluster. The two intermediate waves, i.e., at −0.45 and 1.00 V, can be considered anomalous when compared with the series of regular clusters. Most puzzling is the fact that in conventional systems, the NO^+/NO^0 couple exhibits an electrochemical wave in the range from −0.6 to +0.3 V vs. Ag/Ag^+ [58,59]. It is known that the redox processes are dependent on the nature of the ligands coordinated to the metal centers [60,61]; however, if the redox wave at −0.45 were assigned to the NO^+/NO^0 couple, the next two redox waves of the clusters species would differ by a factor as large as 2.17 V. This interpretation is unlikely,

since there is no precedent for this type of behavior in the chemistry of ruthenium cluster species.

According to the molecular orbital calculations and EPR measurements, there is a strong electronic coupling between the NO ligand and the Ru_3O^+ moiety, where the metal centers are formally in the III, III, III oxidation state. Because of the preferential stabilization of the $Ru_3^{III,III,III}$ state by the electronic mixing with NO ligand, the associated formal redox couples, i.e., E^0(III,III,III/III,III,II) = −0.45 V and E^0(IV,III,III/III,III,III) = 1.00 V, will be shifted to more negative and more positive potentials, respectively, as observed experimentally. In other words, this means that the redox processes involving the NO ligand are shared with the Ru_3O^+ center. Consequently, the electrochemical properties of the $NO^{0/+}$ couple cannot be observed, in separate, as in the conventional NO complexes.

3.7. Visible–UV and FT-IR spectroelectrochemistry

The spectroelectrochemical measurements in the UV–Vis (Fig. 6(a)–(c) and infrared region (Fig. 6(d)–(f)) were carried out within the working range of the gold minigrid electrode (from −2.0 to +1.3 V). In contrast to the typical cluster species [47,62–64], only minor changes in electronic spectra were observed for the $[Ru_3O(NO)]^{2+/+}$ process in the range from 0.00 to +1.10 V (Fig. 6(a)). However, in the FT-IR spectra (Fig. 6(d)) there is a decay of the NO vibrational peak at 1874 cm^{-1} followed by the rise of a less intense peak at 1910 cm^{-1}, indicating that in the oxidized complex, the NO ligand exhibits a predominantly NO^+ character.

Moving down to negative potentials, the UV–Vis spectroelectrochemistry recorded from 0 to −0.80 V showed a decrease of the intracluster band at 543 nm concomitantly with the increase of a broad intracluster band around 700 nm (Fig. 6(b)). Additionally, the intense band at 394 nm in the reduced cluster can be attributed to the characteristic cluster-to-pyridine ring charge-transfer transition in the formal $Ru_3^{III,III,II}$ species [38]. In the corresponding FT-IR spectra (Fig. 6(e)), the shift of ν(NO) from 1874 to 1784 cm^{-1} reflects the influence of π-back donation from the ruthenium center, in the $Ru_3^{III,III,II}$ oxidation state, conveying some NO^- character to this ligand.

Further reduction below −1.0 V produced a red shift of the cluster-to-pyridine charge-transfer band from 394 to 436 nm, and a splitting of the intracluster transition around 700 nm (Fig. 6(c)). This process, however, was found to be irreversible in the time scale of the spectroelectrochemical experiments. In fact, by reversing the potentials from −1.60 to −1.00 V, the initial spectrum at −1.00 V was not regenerated and, instead, the new spectrum was similar to that of conventional reduced clusters containing only N-heterocyclic ligands. Presumably, the second reduction completely populated the antibonding (LUMO) orbital involving strong mixing of cluster-NO, weakening this bonding and releasing

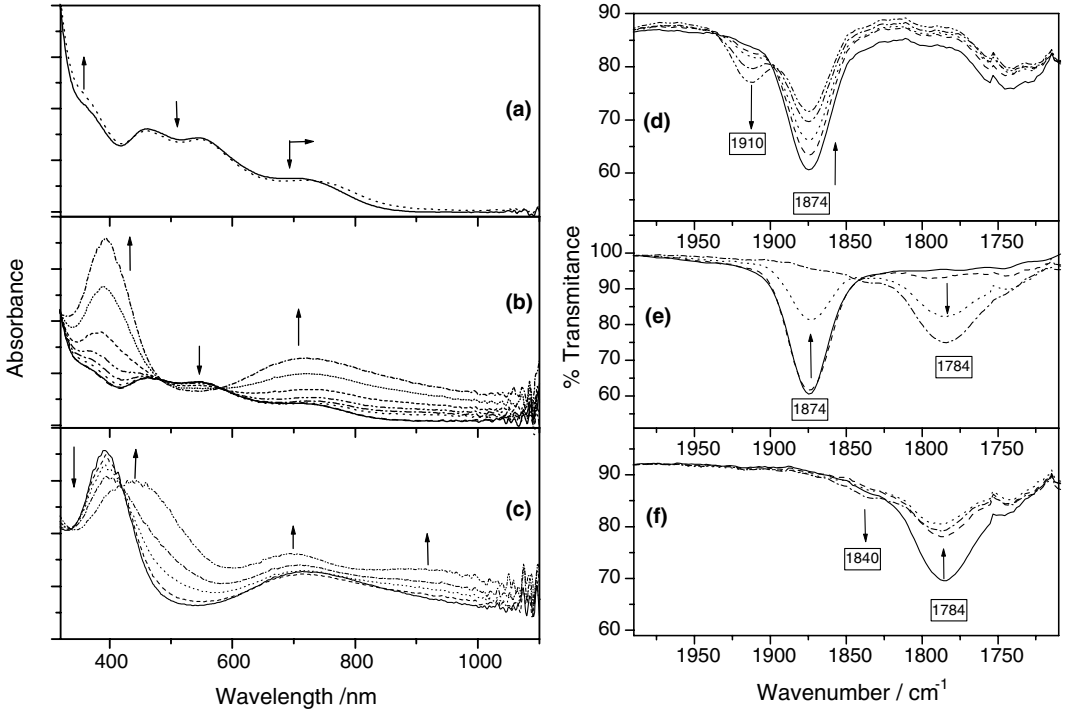

Fig. 6. UV–Vis (a–c) and FT-IR (d–f) spectroelectrochemistry of the 10^{-3} mol L^{-1} $[Ru_3O(CH_3CO_2)_6(pic)_2(NO)]PF_6$ solution in 0.1 mol L^{-1} $TEAClO_4$ (a–c) or $LiClO_4$ (d–f) in acetonitrile. (a) From 0.00 to +1.10 V; (b) from 0.00 to −0.80 V; (c) from −1.00 to −1.40 V; (d) from +0.90 to +1.30 V; (e) from 0.00 to −0.60 V; (f) from −1.00 to −1.30 V.

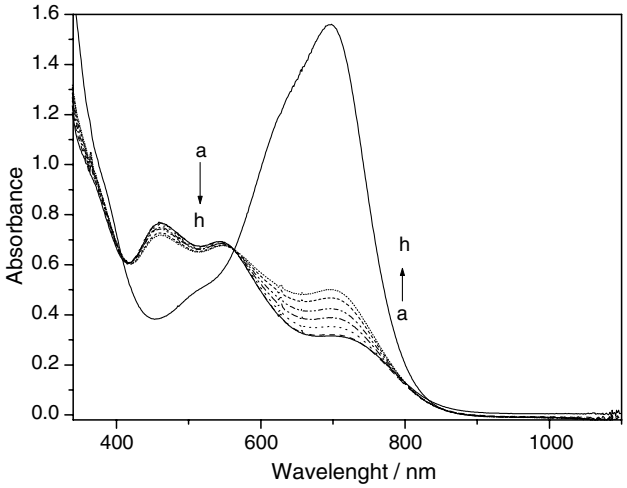

Fig. 7. Electronic spectra of 10^{-4} mol L^{-1} $[Ru_3O(CH_3CO_2)_6(pic)_2(NO)]PF_6$ solution in acetonitrile in the absence of light (a) and irradiated in 468 nm for 5 min (b), 20 min (c), 35 min (d), 50 min (e), 70 min (f), 85 min (g) and (h) after 15 h.

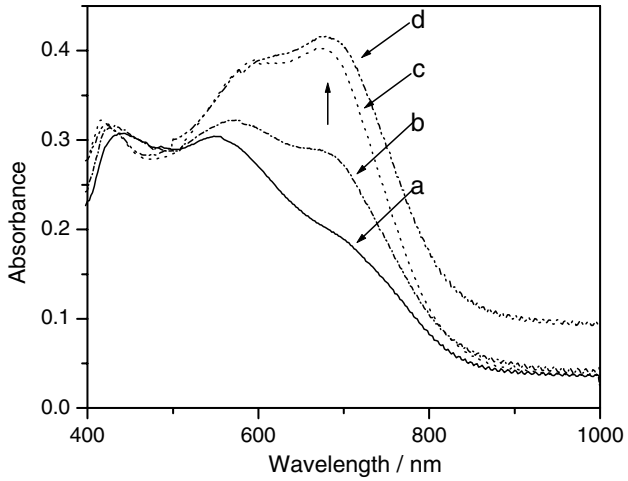

Fig. 8. UV–Vis spectrum of $[Ru_3OAc_6(pic)_2(NO)]PF_6$ suspended in a polyvinyl alcohol film, which was kept on the laboratory bench, after (a) $t = 0$, (b) $t = 1$ week, (c) $t = 2$ weeks, (d) $t = 4$ weeks, of exposure to internal day light and dark night cycles. A control sample kept in the dark exhibited negligible changes during the same period of time.

the NO ligand. The IR spectroelectrochemical data (Fig. 6(f)) are in accord to the explanation above, since as the reduction proceeded the peak intensity at 1784 cm^{-1} decreased. In the expanded spectra only a very weak shoulder was detected at 1870 cm^{-1}, evidencing the released NO molecule remaining in the interfacial double layer.

3.8. Photochemical behavior

The $[Ru_3O(CH_3CO_2)_6(pic)_2(NO)]^+$ cluster is thermally stable but in the presence of light its original violet color slowly changes into deep blue. Irradiation of a cluster solution at 468 nm causes a decrease in the intensity of the bands in 543 and 460 nm, and an increase in the band intensity around 700 nm (Fig. 7). After 15 h of irradiation of a methanol solution, the spectra coincided with that of the starting complex $[Ru_3O(CH_3CO_2)_6(pic)_2(CH_3OH)]^+$, indicating the NO release. The quantum yields ($\phi = 0.038$ at 365 nm and $\phi = 0.019$ at 468 nm) obtained from spectrophotometry were comparable to those of typical NO photoreleasing systems [17,65]. The same behavior was also observed in solid state and in PVA films incorporating this compound (Fig. 8).

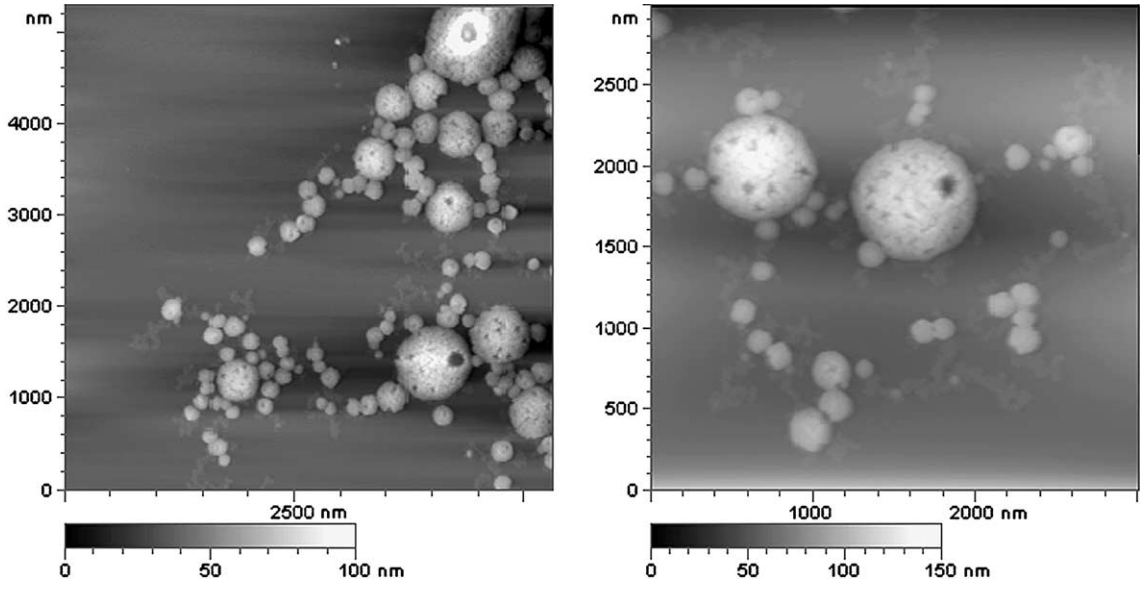

Fig. 9. MAC mode AFM images of $[Ru_3OAc_6(pic)_2(NO)]PF_6$ nanoparticles deposited on mica, showing the round shaped structures with many dispersed holes.

3.9. MAC mode AFM images

As one can see in the AFM images of Fig. 9, the cluster particles generated by the evaporation of the methanol solution on the mica substrate are constituted by variable size, round shaped structures of nanometric size. The most curious point is the presence of a large number of holes. The observed morphology is quite different from those obtained with similar cluster species containing no nitrosyl ligands. Because of this, and of the photochemical sensibility of the nitrosyl-cluster, we believe that such holes may be generated from the NO released from the solid particles. A detailed investigation, using electron microscopy and other SPM techniques is being carried out to elucidate this point.

4. Conclusion

Extending our previous work on the interaction of the pyridine–ruthenium–acetate clusters with NO [39], we have confirmed the existence of a strong Ru–NO electronic coupling, responsible for the loss of the metal and NO ligand identities in the EPR, cyclic voltammetry and FT-IR spectroelectrochemistry results. Such conclusion has been corroborated by semi-empirical theoretical calculations, supporting a predominantly NO^0 character for the nitrosyl ligand in the $[Ru_3O(CH_3CO_2)_6(C_5H_5N)_2(NO)]PF_6$ cluster. NO photoreleasing properties have been observed either in solution or in the solid state, providing a promising system for photodynamic therapy, as well as for the monitoration of light exposure intensities.

Acknowledgments

Financial support from FAPESP, CNPq, RENAMI and IM2C is gratefully acknowledged.

References

[1] E. Culotta, J.D.E. Koshland, Science 258 (1992) 1862.
[2] L.J. Ignarro, Pharm. Res. 6 (1989) 651.
[3] S. Moncada, R.M.J. Palmer, E.A. Higgs, Pharmacol. Rev. 43 (1991) 109.
[4] M.J. Clarke, J.B. Gaul, Struct. Bond. 81 (1993) 147.
[5] A.R. Butler, D.L.H. Williams, Chem. Soc. Rev. (1993) 233.
[6] M. Fontecave, J.-L. Pierre, Bull. Soc. Chim. Fr. 131 (1994) 620.
[7] R.J.P. Williams, Chem. Soc. Rev. (1996) 77.
[8] D.A. Wink, J.B. Mitchell, Free Radic. Biol. Med. 25 (1998) 434.
[9] S.P. Fricker, Platinum Metals Rev. 39 (1995) 150.
[10] N. Bettache, T. Carter, J.E.T. Corrie, D. Ogden, D.R. Trentham, Method Enzymol. 268 (1996) 266.
[11] S.P. Fricker, E. Slade, N.A. Powell, O.J. Vaugham, G.R. Henderson, B.A. Murrer, I.L. Megson, S.K. Bisland, F.W. Flitney, Br. J. Pharmacol. 122 (1997) 1441.
[12] T.D. Carter, N. Bettache, D. Ogden, Br. J. Pharmacol. 122 (1997) 971.
[13] Y. Chen, R.E. Shepherd, J. Inorg. Biochem. 68 (1997) 183.
[14] N.A. Davies, M.T. Wilson, E. Slade, S.P. Fricker, B.A. Murrer, N.A. Powell, G.R. Henderson, Chem. Commun. (1997) 47.
[15] P.C. Ford, J. Bourassa, K. Miranda, B. Lee, I. Lorkovic, S. Boggs, S. Kudo, L. Laverman, Coord. Chem. Rev. 171 (1998) 185.
[16] K. Szacilowski, W. Macyk, G. Stochel, Z. Stasicka, S. Sostero, O. Traverso, Coord. Chem. Rev. 208 (2000) 277.
[17] C.F. Works, P.C. Ford, J. Am. Chem. Soc. 122 (2000) 7592.
[18] L.G.F. Lopes, A. Wieraszko, Y. El-Sherif, M.J. Clarke, Inorg. Chim. Acta 312 (2001) 15.
[19] V. Togniolo, R.S. Silva, A.C. Tedesco, Inorg. Chim. Acta 316 (2001) 7.
[20] A. Wanat, T. Schneppensieper, A. Karocki, G. Stochel, R. Eldik, J. Chem. Soc., Dalton Trans. (2002) 941.
[21] M.G. Sauaia, R.R. Santana, Transition Met. Chem. 28 (2003) 254.
[22] M.G. Sauaia, F.S. Oliveira, A.C. Tedesco, R.S. Silva, Inorg. Chim. Acta 355 (2003) 191.
[23] B.R. Cameron, M.C. Darkes, H. Yee, M. Olsen, S.P. Fricker, R.T. Skerlj, G.J. Bridger, N.A. Davies, M.T. Wilson, D.J. Rose, J. Zubieta, Inorg. Chem. 42 (2003) 1868.
[24] E. Tfouni, M. Krieger, B.R. McGarvey, D.W. Franco, Coord. Chem. Rev. 236 (2003) 57.
[25] J.M. Slocik, R.E. Shepherd, Inorg. Chim. Acta 311 (2000) 80.
[26] J.M. Slocik, M.S. Ward, K.V. Somayajula, R.E. Shepherd, Transition Met. Chem. 26 (2001) 351.
[27] J.M. Slocik, K.V. Somayajula, R.E. Shepherd, Inorg. Chim. Acta 320 (2001) 148.
[28] J.M. Slocik, M.S. Ward, R.E. Shepherd, Inorg. Chim. Acta 317 (2001) 290.
[29] T.W. Stringfield, K.V. Somayajula, D.C. Muddiman, J.W. Flora, R.E. Shepherd, Inorg. Chim. Acta 343 (2003) 317.
[30] M.S. Ward, F. Lin, R.E. Shepherd, Inorg. Chim. Acta 343 (2003) 231.
[31] Y. Chen, R.E. Shepherd, Inorg. Chim. Acta 343 (2003) 281.
[32] R.E. Shepherd, J.M. Slocik, T.W. Stringfield, K.V. Somayajula, A.A. Amoscato, Inorg. Chim. Acta 357 (2004) 965.
[33] J.H. Enemark, R.D. Feltham, Coord. Chem. Rev 13 (1974) 339.
[34] R. Eisenberg, C.D. Meyer, Acc. Chem. Res. 8 (1975) 26.
[35] F. Bottomley, Coord. Chem. Rev. 26 (1978) 7.
[36] B.L. Westcott, J.H. Enemark, Transition Metal Nitrosyls, Wiley, New York, 1999.
[37] Y. Chen, F. Lin, R.E. Shepherd, Inorg. Chem. 38 (1999) 973.
[38] H.E. Toma, K. Araki, A.D.P. Alexiou, S. Nikolaou, S. Dovidauskas, Coord. Chem. Rev. 219–221 (2001) 225.
[39] H.E. Toma, A.D.P. Alexiou, S. Dovidauskas, Eur. J. Inorg. Chem. (2002) 3010.
[40] D.T. Sawyer, J.L. Roberts, Experimental Electrochemistry for Chemists, Wiley, New York, 1974.
[41] J.A. Baumann, D.J. Salmon, S.T. Wilson, T.J. Meyer, W.E. Hatfield, Inorg. Chem. 17 (1978) 3342.
[42] L.V. Natarajan, M. Robinson, R.E. Blankenship, J. Chem. Educ. 60 (1983) 241.
[43] M. Abe, Y. Sasaki, Y. Yamada, K. Tsukahara, S. Yano, T. Yamaguchi, M. Tominaga, I. Taniguchi, T. Ito, Inorg. Chem. 35 (1996) 6724.
[44] K. Ota, H. Sasaki, T. Matsui, T. Hamaguchi, T. Yamaguchi, T. Ito, H. Kido, C.P. Kubiak, Inorg. Chem. 38 (1999) 4070.
[45] M. Abe, Y. Sasaki, A. Nagasawa, T. Ito, Bull. Chem. Soc. Jpn. 65 (1992) 1411.
[46] H.E. Toma, A.D.P. Alexiou, J. Braz. Chem. Soc. 6 (1995) 267.
[47] H.E. Toma, A.D.P. Alexiou, J. Chem. Res. (S) (1995) 134.
[48] A.D.P. Alexiou, H.E. Toma, J. Chem. Res. (S) (1997) 338.

[49] H.E. Toma, A.D.P. Alexiou, S. Nikolaou, S. Dovidauskas, Magn. Reson. Chem. 37 (1999) 322.
[50] S. Dovidauskas, H.E. Toma, K. Araki, H. Sacco, Y. Iamamoto, Inorg. Chim. Acta 305 (2000) 206.
[51] S. Dovidauskas, K. Araki, H.E. Toma, J. Porphyrins Phthalocyanines 4 (2000) 727.
[52] K. Araki, S. Dovidauskas, H. Winnischofer, A.D.P. Alexiou, H.E. Toma, J. Electroanal. Chem. 498 (2001) 152.
[53] S. Nikolaou, M. Uemi, H.E. Toma, Spectrosc. Lett. 34 (2001) 267.
[54] J.A. Iggo, NMR Spectroscopy in Inorganic Chemistry, Oxford University Press, New York, 1999.
[55] M. Abe, A. Sato, T. Inomata, T. Kondo, K. Uosaki, Y. Sasaki, J. Chem. Soc., Dalton Trans. (2000) 2693.
[56] A. Sato, M. Abe, T. Inomata, T. Kondo, S. Ye, K. Uosaki, Y. Sasaki, Phys. Chem. Chem. Phys. 3 (2001) 3420.
[57] F.A. Cotton, J.G. Norman Jr., Inorg. Chim. Acta 6 (1972) 411.
[58] E.S. Dodsworth, A.A. Vleck, A.B.P. Lever, Inorg. Chem. 33 (1994) 1045.
[59] L.G.F. Lopes, M.G. Gomes, S.S.S. Borges, D.W. Franco, Aust. J. Chem. 51 (1998) 865.
[60] H.E. Toma, C.J. Cunha, C. Cipriano, Inorg. Chim. Acta 154 (1988) 63.
[61] A.D.P. Alexiou, H.E. Toma, J. Chem. Res. (S) (1993) 464.
[62] H.E. Toma, C.J. Cunha, Can. J. Chem. 67 (1989) 1632.
[63] H.E. Toma, C. Cipriano, J. Electroanal. Chem. 263 (1989) 313.
[64] M. Abe, Y. Sasaki, Y. Yamada, K. Tsukahara, S. Yano, T. Ito, Inorg. Chem. 34 (1995) 4490.
[65] H. Kunkely, A. Vogler, Inorg. Chim. Acta 346 (2003) 275.